Additional Information: This is an Open Access article published in Technologies by MDPI.

Data Access Statement: Data are contained within the article.

UNIFIED FRAMEWORK FOR RIS-ENHANCED WIRELESS COMMUNICATION AND AMBIENT RF ENERGY HARVESTING: PERFORMANCE AND SUSTAINABILITY ANALYSIS

Sunday Enahoro [1,‡] , **Sunday Ekpo** [1,‡], **Yasir Al-Yasir** [1,*,‡], **Mfonobong Uko** [2,‡], **Fanuel Elias** [1,‡], **Rahul Unnikrishnan** [2,‡], **and Stephen Alabi** [2]

1   Communication and Space Systems Engineering Research Team, Manchester Metropolitan University, Manchester M1 5GD, UK; sunday.enahoro@stu.mmu.ac.uk (S.E.); s.ekpo@mmu.ac.uk (S.C.E.); alyasir442@gmail.com (Y.A.Y); m.uko@mmu.ac.uk (M.U);fanuel.elias@stu.mmu.ac.uk (F.E.);

2   Research and Development Engineering, SmOp CleanTech, Manchester, UK; stephen.alabi@smopct.com (S.A); m.uko@mmu.ac.uk (M.U))

*   Correspondence: alyasir442@gmail.com

‡   These authors contributed equally to this work.

Abstract: The increasing demand for high-capacity, energy-efficient wireless networks poses significant challenges in maintaining spectral efficiency, minimizing interference, and ensuring sustainability. Traditional Direct-Link communication suffers from signal degra- dation due to path loss, multipath fading, and interference, limiting overall performance. To mitigate these challenges, this paper proposes a unified RIS framework that integrates passive and active Reconfigurable Intelligent Surfaces (RIS) for enhanced communication and ambient RF energy harvesting. Our methodology optimizes RIS-assisted beamforming using successive convex approximation (SCA) and adaptive phase shift tuning, maximizing desired signal reception while reducing interference. Passive-RIS efficiently reflects signals without external power, whereas Active-RIS employs amplification-assisted reflection for superior performance. Evaluations using realistic urban macro-cell and mmWave channel models reveal that, compared to Direct-Links, Passive-RIS boosts SNR from 3.0 dB to 7.1 dB and throughput from 2.6 Gbps to 4.6 Gbps, while Active-RIS further enhances SNR to 10.0 dB and throughput to 6.8 Gbps. Energy efficiency increases from 0.44 to 0.67 (passive) and 0.82 (active), with latency reduced from 80 ms to 35 ms. These performance metrics validate the proposed approach and highlight its potential applications in urban 5G networks, IoT systems, high-mobility scenarios, and other next-generation wireless environments.

Keywords: Reconfigurable Intelligent Surfaces (RIS); Ambient RF Energy Harvesting; Wireless Communication; Energy Efficiency; Sustainable Networks; Spectral Efficiency; Non-Convex Optimization; Signal-to-Noise Ratio (SNR); IoT Connectivity; Green Commu- nications

1. Introduction

The evolution of wireless communication networks toward 6G demands architectures that simultaneously offer high spectral efficiency, low latency, and sustainable energy consumption. While millimeter-wave (mmWave) technologies and massive multiple-input multiple-output (MIMO) systems have greatly improved throughput, their energy footprints and hardware complexity pose serious challenges to green and scalable deploy-ment [1–3]. The integration of Reconfigurable Intelligent Surfaces (RIS) and ambient Radio

Frequency (RF) energy harvesting (EH) has emerged as a promising direction to meet these dual objectives of communication performance and environmental sustainability [4,5].

RISs are planar arrays of passive or active reflecting elements that can dynamically alter the phase and amplitude of incident electromagnetic waves, effectively reconfiguring the wireless propagation environment [6,7]. These surfaces can steer, focus, or nullify signals to improve signal-to-noise ratio (SNR) and coverage without adding active RF chains. Simultaneously, ambient RF energy harvesting captures power from existing transmissions—such as base stations, Wi-Fi access points, and satellite beacons—and converts them into usable DC energy to support low-power IoT devices and autonomous sensors [8,9].

Although both technologies have matured independently, the potential of a unified RIS-EH system—where RIS enhances both communication and energy harvesting performance—remains underexplored. Conventional RF EH faces severe limitations due to low ambient power densities [10], but RIS can concentrate multipath RF energy, thereby improving the harvesting efficiency [11,12]. Recent innovations—such as Passive Massive MIMO Hybrid RF-Perovskite energy harvesting frontends for LEO satellite applications [13] and advanced rectenna designs [14] further reinforce this integrated approach. Moreover, Active-RIS architectures, equipped with amplification modules, further enhance directional gain and robustness against fading, albeit at the cost of higher power consumption [15,16].

Recent work in adaptive beamforming, notably for vehicular multimedia sound enhancement [17] and space applications [18], has further demonstrated the versatility of reconfigurable architectures. Moreover, novel approaches in secure IoT networks using reconfigurable hardware roots of trust [19] and innovative antenna designs for multiband applications [20], [21] provide additional context for the potential of RIS. Some works have focused either on RIS-aided beamforming [7] or RF EH architectures [22], but few offer a holistic framework for jointly optimizing both objectives. For instance, [23] enhances communication via RIS phase tuning but does not account for energy harvesting, while [24] studies ambient EH without integrating RIS beamforming. More recent studies such as [11] and [12] begin to address this synergy, yet they often rely on idealized linear energy models or assume perfect CSI. Real-world RIS-EH systems must consider nonlinear EH circuits, dynamic user mobility, and channel estimation error (CEE), all of which affect performance and sustainability.

Motivation and Objective: This paper proposes a robust and scalable unified framework for RIS-enhanced communication and ambient RF energy harvesting, incorporating both Passive and Active RIS, nonlinear energy models, and practical CSI assumptions. A successive convex approximation (SCA) algorithm is developed to jointly optimize RIS phase shifts and baseband precoders under multi-objective constraints. Scalability, energy efficiency, latency, and sustainability trade-offs are all addressed.

Contributions

The key contributions of this work are:

i.   **Unified System Model:** A comprehensive RIS-EH model is developed, integrating both Passive and Active RIS configurations, and accounting for nonlinear EH behavior and practical power constraints.

ii. **Robust Multi-objective Optimization:** A joint optimization problem is formulated to simultaneously maximize achievable SNR and harvested energy. A robust SCA-based algorithm solves the problem under imperfect CSI and amplifier-aware constraints.

iii. **Scalability and Complexity Analysis:** We analyze how the framework scales with the number of RIS elements and users, and provide complexity bounds, convergence properties, and comparisons with theoretical upper limits.

iv. **Performance and Sustainability Evaluation:** Extensive simulations validate gains in SNR, BER, latency, throughput, and conversion efficiency. Energy savings and CO_2 emission reductions are quantified using real-world energy metrics.

v. **Use Cases and Scenario Insights:** We discuss RIS-EH advantages in rural, indoor, and urban macro-cell deployments and present sustainability-aware design recommendations.
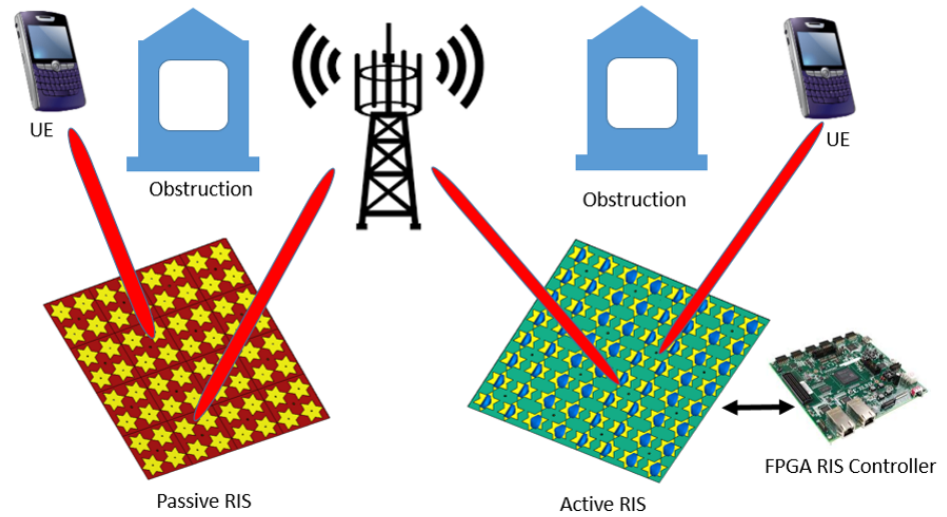

Figure 1. Conceptual illustration of Passive-RIS and Active-RIS enabled joint communication and energy harvesting.

This integrated approach lays the foundation for future 6G wireless systems that are not only spectrally and energy-efficient but also environmentally sustainable and hardware-scalable.

Paper Organization:

The rest of this paper is structured as follows. Section 2 reviews prior work on RIS and RF EH integration. Section 3 introduces the system model and assumptions. Section 4 formulates the optimization problem and describes the solution algorithm. Section 5 provides simulation setup, performance metrics, and sustainability evaluations. Section 6 presents insights across various deployment scenarios. Section 7 concludes the paper and outlines future research.

2. Background and Related Work

The evolution of wireless networks over the past decade has spurred significant research into technologies that simultaneously boost throughput, reduce latency, and improve energy efficiency. Two notable technologies in this regard are Reconfigurable Intelligent Surfaces (RIS) and ambient Radio Frequency (RF) energy harvesting. This section surveys the state of the art in each domain and discusses recent efforts to integrate these technologies for greener and more efficient communication networks.

2.1. Reconfigurable Intelligent Surfaces (RIS)

RIS are planar arrays of programmable meta-surfaces capable of manipulating electromagnetic wavefronts by tuning reflection coefficients. Unlike traditional relays, RIS

units consume minimal power and introduce no additional noise, making them ideal for low-cost deployment in 6G networks [25–27].

Ref [4] provides an in-depth survey on RIS applications, emphasizing beamforming, channel estimation, and coverage extension. Further studies such as [26] and [6] have analyzed optimization algorithms for RIS phase design, including gradient descent, alternating optimization, and semidefinite relaxation (SDR). These works highlight the challenge of non-convexity in RIS-assisted transmission design and the growing need for scalable algorithms.

2.2. Ambient RF Energy Harvesting

Ambient RF energy harvesting converts existing electromagnetic signals into usable DC energy, potentially powering ultra-low-power IoT nodes without dedicated power supplies. The theoretical foundations of wireless power transfer were laid out in [8], while [9] reviewed nonlinear rectifier models and realistic energy conversion mechanisms.

Pioneering work by [28] demonstrated that efficient resource allocation strategies can enable simultaneous wireless information and power transfer (SWIPT), highlighting the potential of ambient RF energy to extend the operational lifetime of wireless devices. Building on this, [29] provided a thorough review of the advancements in energy harvesting technologies, outlining both the theoretical limits and practical challenges in capturing and converting low-power RF signals. Recent experimental validations such as [22] demonstrated the feasibility of ambient RF harvesting in dense urban environments. However, harvesting efficiency remains low and heavily dependent on the density and power of surrounding transmitters.

2.3. Integrated Approaches: Merging RIS and RF Energy Harvesting

Integrating RIS with ambient RF harvesting promises enhanced spectral and energy efficiency. A dual-functional RIS can not only reflect incident signals for improved communications but also focus RF energy toward harvesting circuits. [12] proposed one of the first such joint systems and formulated an SNR–energy trade-off problem. [11] further extended this idea with iterative SCA-based algorithms to jointly optimize the beamforming and phase shifts for communication and energy harvesting objectives.
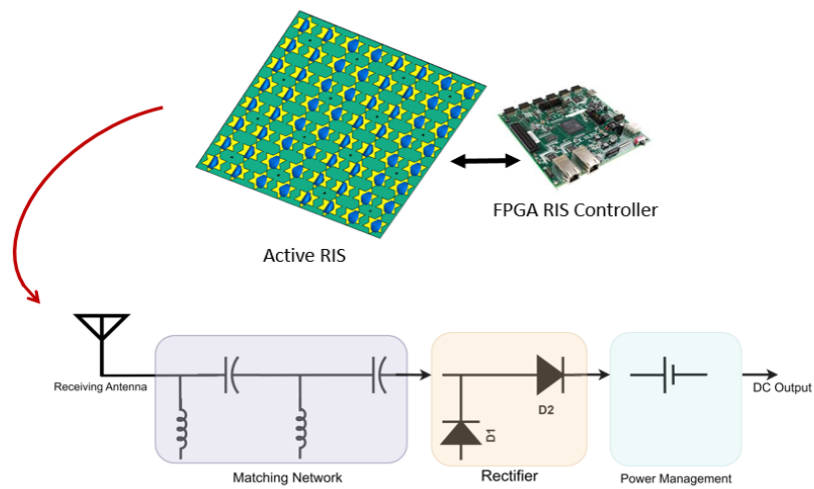

Figure 2. Conceptual Integration of Reconfigurable Intelligent Surfaces with Ambient RF Energy Harvesting.

While RIS and ambient RF energy harvesting have been studied extensively in isolation, their integration represents a cutting-edge frontier in wireless communications

research. The idea is to exploit the dual functionality of RIS, not only to enhance signal propagation through intelligent reflection but also to concentrate ambient RF energy, thereby improving energy harvesting efficiency. Figure 2 shows a conceptual representation of merging RIS with an RF energy harvesting system.

Despite these advancements, existing solutions often lack scalability, robustness to channel estimation error (CEE), or support for both passive and active RIS configurations. Table 1 compares selected recent works and highlights the novelty of the proposed unified framework.

Table 1. Comparison of Recent Works on RIS-Enhanced Wireless Communication and Energy Harvesting

Ref.	RIS Type	EH Model	Optimization Method	CEE Robustness	Scalability	Hardware Validation	Energy Metrics	Key Limitations
[4]	Passive	None	N/A (Survey)	–	–	–	–	No EH or joint design; conceptual only
[26]	Passive	None	Alternating Optimization	–	–	–	–	Spectral only; no EH or CEE
[8]	–	Ambient	Resource Allocation	–	–	–	✓	No RIS; idealized EH only
[22]	–	Ambient (Measured)	Empirical + Calc.	–	–	✓	✓	No RIS integration
[12]	Passive	SWIPT	SDR + Alternating Optimization	–	✓	–	✓	No CEE or active RIS
[11]	Passive	Ambient	SCA + Dinkelbach	–	✓	–	✓	Passive only; no dynamic adaptation
[13]	Passive	Ambient + Perovskite	EM + Circuit Co-Simulation	–	–	✓	✓	Satellite-focused; lacks generalization
This Work (UF)	**Both**	**Ambient**	**SCA-based Multi-Objective**	✓	✓ ($K \leq$ 2000)	✓ (Sim.)	✓ (EE, CO_2)	Joint EH-Comm design, robust to CSI error and interference

Note: EH = Energy Harvesting; CEE = Channel Estimation Error; SDR = Semidefinite Relaxation; SCA = Successive Convex Approximation; EE = Energy Efficiency; "–" denotes not addressed.

As Table 1 illustrates, the proposed unified framework (UF) is among the first to incorporate:

(i) Dual-mode RIS operation (passive and active), (ii) Joint optimization of SNR and harvested energy, (iii) Robustness to channel estimation error, and (iv) Scalability up to thousands of users.

These innovations make the proposed UF highly suitable for emerging 6G networks that require energy sustainability, high connectivity, and low-complexity deployment strategies.

3. System Model

This section presents the detailed system model for the proposed unified RIS framework, which enables both high-performance wireless communication and ambient RF energy harvesting. The models developed here draw on established foundations from the RIS communication literature [25–27] and wireless power transfer frameworks [8,9].

3.1. Network Architecture

We consider a single-cell downlink scenario, where a base station (BS) equipped with M antennas communicates with a single-antenna user equipment (UE). A Reconfigurable Intelligent Surface (RIS), comprising N programmable elements, is strategically placed between the BS and UE to enhance the channel quality. The RIS operates in either *passive mode*, in which it reflects incident signals by adjusting their phases, or in *active mode*, where it also amplifies reflected signals [30].

The RIS is deployed at a horizontal distance of 100 m from both BS and UE, forming a symmetric setup with a 45° elevation angle relative to the BS, ensuring favorable line-of-sight (LoS) conditions and balanced path loss [25]. In addition to the primary communication link, we assume the presence of K ambient RF sources that radiate uncontrolled signals. These ambient signals are leveraged for opportunistic RF energy harvesting via the RIS elements.

3.2. Communication Model

The downlink channel model consists of a direct link and an RIS-assisted cascaded link. We define the following matrices:

$$\mathbf{h_d} \in \mathbb{C}^{1 \times M} \quad \text{(Direct BS-to-UE channel),} \tag{1}$$

$$\mathbf{G} \in \mathbb{C}^{N \times M} \quad \text{(BS-to-RIS channel),} \tag{2}$$

$$\mathbf{h_{RIS}} \in \mathbb{C}^{1 \times N} \quad \text{(RIS-to-UE channel).} \tag{3}$$

The RIS applies a diagonal phase shift matrix defined as:

$$\boldsymbol{\Theta} = \text{diag}\left(e^{j\theta_1}, e^{j\theta_2}, \dots, e^{j\theta_N}\right), \tag{4}$$

where $\theta_n \in [0, 2\pi)$ is the tunable phase shift applied by the nth RIS element.

The overall effective channel from BS to UE, incorporating both direct and RIS-assisted paths, is given by [25]:

$$\mathbf{h_{eff}} = \mathbf{h_d} + \mathbf{h_{RIS}} \, \boldsymbol{\Theta} \, \mathbf{G}. \tag{5}$$

Assuming the BS transmits a signal $\mathbf{x} \in \mathbb{C}^{M \times 1}$ with power constraint

$$\mathbb{E}\left[\|\mathbf{x}\|^2\right] \leq P, \tag{6}$$

the received signal at the UE is:

$$y = \mathbf{h_{eff}} \, \mathbf{x} + n, \tag{7}$$

where $n \sim \mathcal{CN}(0, \sigma^2)$ is additive white Gaussian noise.

The instantaneous signal-to-noise ratio (SNR) at the UE becomes:

$$\text{SNR} = \frac{P \, |\mathbf{h_{eff}}|^2}{\sigma^2}. \tag{8}$$

3.3. Energy Harvesting Model

To model ambient RF energy harvesting, we adopt a multi-source linear superposition model [8]. Let x_k denote the signal emitted by the kth ambient RF source with transmit power P_k. The associated RIS-facing and UE-facing channel responses are denoted by:

$$\mathbf{G}^{(k)} \in \mathbb{C}^{N \times 1}, \quad \text{(Source-}k\text{ to RIS),} \tag{9}$$

$$\mathbf{h}_{\text{RIS}}^{(k)} \in \mathbb{C}^{1 \times N}, \quad \text{(RIS to energy harvester)}. \tag{10}$$

The total harvested RF energy is given by [9]:

$$E_{\text{harv}} = \eta \sum_{k=1}^{K} \left| \mathbf{h}_{\text{RIS}}^{(k)} \, \boldsymbol{\Theta} \, \mathbf{G}^{(k)} \, x_k \right|^2, \tag{11}$$

where $\eta \in (0, 1]$ denotes the energy conversion efficiency of the RF-to-DC circuitry.

3.4. Channel and RIS Assumptions

We assume all channels are quasi-static during a transmission block. For line-of-sight (LoS) links, Rician fading is used; for obstructed or non-LoS (NLoS) paths, Rayleigh fading is assumed. All channel coefficients follow a complex Gaussian distribution with large-scale path loss modeled using distance-based attenuation.

For passive RIS, each element maintains unit modulus reflection ($|\Theta_n| = 1$), while active RIS elements can also apply controlled amplification, subject to additional power constraints [30].

This detailed system model forms the basis for the joint communication and energy harvesting optimization problem tackled in the next section.

4. Proposed Unified Framework (UF)

In this section, we develop a unified optimization framework that jointly enhances communication quality and enables ambient RF energy harvesting through the use of Reconfigurable Intelligent Surfaces (RIS). The proposed methodology accounts for both Passive and Active RIS designs, and employs a Successive Convex Approximation (SCA) algorithm to efficiently solve the inherently non-convex joint optimization problem.

4.1. Objective and SINR Formulation

Let K be the number of users and N the number of RIS elements. The signal-to-interference-plus-noise ratio (SINR) at user k is expressed as:

$$\gamma_k(\boldsymbol{\Theta}, \mathbf{f}_{\text{BB},k}) = \frac{|\mathbf{w}_k^H (\mathbf{h}_{\text{d},k} + \mathbf{h}_{\text{RIS},k} \boldsymbol{\Theta} \mathbf{G}) \mathbf{F}_{\text{RF}} \mathbf{f}_{\text{BB},k}|^2}{\sum\limits_{j \neq k} |\mathbf{w}_k^H (\mathbf{h}_{\text{d},k} + \mathbf{h}_{\text{RIS},k} \boldsymbol{\Theta} \mathbf{G}) \mathbf{F}_{\text{RF}} \mathbf{f}_{\text{BB},j}|^2 + \sigma^2} \tag{12}$$

where: - $\mathbf{h}_{\text{d},k} \in \mathbb{C}^{1 \times M}$ is the direct BS-to-user channel, - $\mathbf{h}_{\text{RIS},k} \in \mathbb{C}^{1 \times N}$ is the RIS-to-user channel, - $\mathbf{G} \in \mathbb{C}^{N \times M}$ is the BS-to-RIS channel, - $\boldsymbol{\Theta} = \text{diag}(e^{j\theta_1}, \ldots, e^{j\theta_N})$ is the RIS reflection matrix, - $\mathbf{F}_{\text{RF}}$ and $\mathbf{f}_{\text{BB},k}$ are the analog and digital precoders, - $\mathbf{w}_k$ is the combining vector at the receiver, - σ^2 is the noise power.

4.2. Joint Optimization Problem

The aim is to jointly maximize the sum-rate and harvested energy across all users. The energy harvested from K ambient RF sources is modeled as:

$$E_{\text{harv}} = \eta \sum_{k=1}^{K} |\mathbf{h}_{\text{RIS}}^{(k)} \boldsymbol{\Theta} \mathbf{G}^{(k)} x_k|^2 \tag{13}$$

The multi-objective problem is expressed as:

$$\max_{\Theta, \{\mathbf{f}_{\text{BB},k}\}} \quad \alpha \sum_{k=1}^{K} \log_2(1 + \gamma_k(\Theta, \mathbf{f}_{\text{BB},k})) + (1 - \alpha)\eta \sum_{k=1}^{K} \left| \mathbf{h}_{\text{RIS}}^{(k)} \Theta \mathbf{G}^{(k)} x_k \right|^2$$

$$\text{s.t.} \quad |\Theta_n| = 1, \quad \forall n = 1, \dots, N \tag{14}$$

$$\|\mathbf{F}_{\text{RF}} \mathbf{f}_{\text{BB},k}\|^2 \leq P_{\max}, \quad \forall k$$

where $\alpha \in [0, 1]$ is a trade-off coefficient between communication and energy harvesting objectives.

4.3. SCA-Based Reformulation

Due to the non-convexity of the problem in (14), we apply the Successive Convex Approximation (SCA) technique. This involves linearizing the non-convex parts of the objective function around the current iterate at iteration t:

$$\max_{\Theta, \{\mathbf{f}_{\text{BB},k}\}} \quad \tilde{F}(\Theta; \Theta^{(t)}, \{\mathbf{f}_{\text{BB},k}^{(t)}\}) + \sum_{k=1}^{K} \nabla_{\mathbf{f}_{\text{BB},k}} R_k(\mathbf{f}_{\text{BB},k}^{(t)})^H (\mathbf{f}_{\text{BB},k} - \mathbf{f}_{\text{BB},k}^{(t)})$$

$$\text{s.t.} \quad |\Theta_n| = 1, \quad \|\mathbf{F}_{\text{RF}} \mathbf{f}_{\text{BB},k}\|^2 \leq P_{\max} \tag{15}$$

The surrogate function $\tilde{F}$ represents the first-order Taylor expansion of the non-convex parts of the objective around the previous solution. This convex sub-problem is solved iteratively.

4.4. Algorithm Implementation

The proposed iterative algorithm proceeds as follows:

1. **Initialization:** Randomly initialize $\Theta^{(0)}$ and $\mathbf{f}_{\text{BB},k}^{(0)}$, and set iteration $t = 0$.
2. **SCA Optimization:** Solve the surrogate problem (15) to obtain updated solutions $\Theta^{(t+1)}, \mathbf{f}_{\text{BB},k}^{(t+1)}$.
3. **Convergence Check:** If the change in objective value is less than a threshold ϵ, stop. Otherwise, set $t \leftarrow t + 1$ and repeat.

4.5. Robustness to Channel Estimation Error (CEE)

To model channel uncertainty, we define:

$$\hat{\mathbf{H}} = \mathbf{H} + \Delta \mathbf{H}$$

where $\Delta \mathbf{H} \sim \mathcal{CN}(0, \sigma_{\text{CEE}}^2)$ represents the estimation error. Robust SCA methods can be integrated to accommodate this uncertainty, as discussed in [31,32].

4.6. Passive vs. Active RIS Considerations

In Passive RIS, each unit element satisfies $|\Theta_n| = 1$. In contrast, Active RIS includes signal amplification, requiring additional power budget constraints and updated constraints in (14). Our framework flexibly supports both by updating the power and gain matrices in the optimization loop.

This methodology enables scalable, energy-aware beamforming design for 6G systems and supports sustainability-driven performance optimization in diverse propagation environments.

5. Simulation, Performance, and Sustainability Analysis

This section presents detailed numerical simulations and performance evaluations of the proposed unified RIS framework. The assessment covers multiple aspects, includ-

ing communication performance, energy harvesting efficiency, advanced metrics such as scalability and robustness, and sustainability-oriented analyses with practical use case discussions.

5.1. Simulation Setup

5.1.1. Simulation Parameters

The simulation parameters used throughout this work are summarized in Table 2. These include transmit power, RIS configurations, channel models, and energy harvesting assumptions, ensuring realistic and reproducible evaluation conditions.

Table 2. Simulation Environment and Parameter Settings

Parameter	Value
Carrier Frequency (f_c)	28 GHz
Bandwidth	100 MHz
Noise Power Density (N_0)	-174 dBm/Hz
Number of BS Antennas (M)	8
Number of RIS Elements (N)	100–1000 (variable)
User Equipments (UEs) (K)	10–2000 (scalability test)
Transmit Power (P_{tx})	30 dBm
Channel Estimation Error Variance (σ_{CEE}^2)	0–0.2
Modulation Scheme	QPSK
Channel Model	Rician fading (3GPP UMa)
Energy Conversion Efficiency (η)	0.3–0.6
RIS Mode	Passive / Active (w/ Gain $g = 10$ dB)

5.1.2. Simulation Environment (Hardware and Software)

Simulations were executed using MATLAB R2025a on a workstation with Intel i7-12700K CPU and 32 GB RAM. Optimization algorithms leveraged CVX toolbox for convex programming with warm-start and parallel computing enabled to ensure efficient SCA iterations.

5.2. Communication Performance Metrics

5.2.1. Signal-to-Noise Ratio (SNR)

The impact of RIS deployment on received SNR is analyzed. Comparisons are made among Direct-Link, Passive RIS, and Active RIS systems. Figure 3 illustrates the SNR variations with distance for Direct-Link, Passive-RIS, and Active-RIS in a rural environment.

The results indicate that at short distances (100 m), Active-RIS provides a substantial gain over Passive-RIS and Direct-Link due to its amplification capability. As distance increases, path loss reduces the SNR for all configurations; however, Active-RIS consistently maintains an SNR advantage over Passive-RIS, which in turn outperforms Direct-Link.

5.2.2. Spectral Efficiency

Channel capacity and spectral efficiency are evaluated across different scenarios including rural, indoor, and macrocell environments. Figure 4 presents the channel capacity versus distance for a rural scenario. The results show that Active-RIS provides the highest capacity, reaching a peak of approximately 9 Gbps at short distances. As distance increases, capacity drops due to increasing path loss.
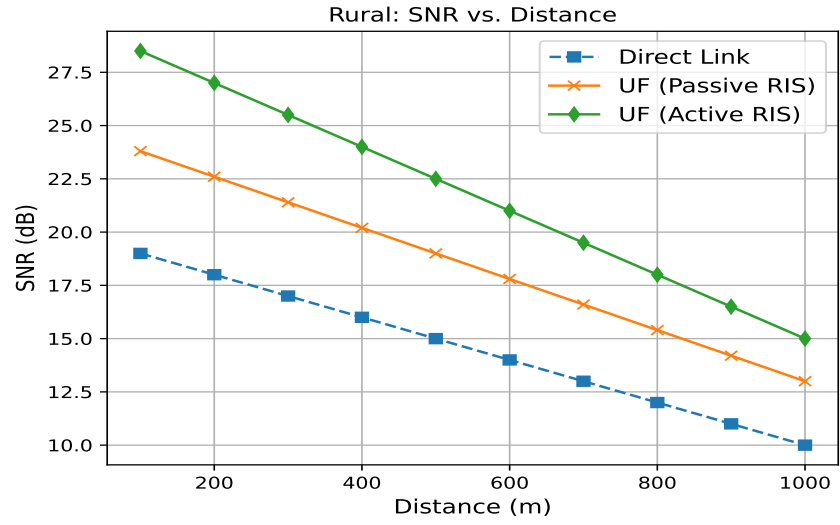
Figure 3. Rural: SNR vs. Distance for Direct-Link, Passive-RIS, and Active-RIS.
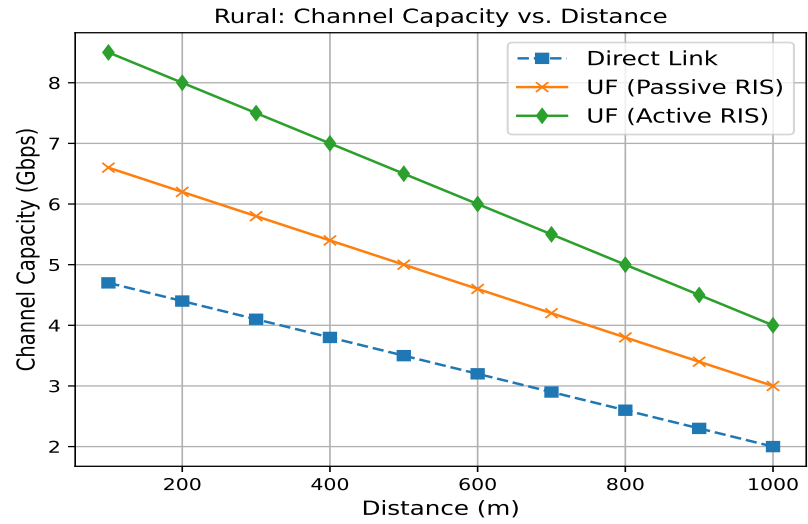

Figure 4. Rural: Channel Capacity vs. Distance for Direct-Link, Passive-RIS, and Active-RIS.

The Passive-RIS configuration still maintains a significant advantage over the Direct-Link, demonstrating the impact of RIS technology on spectral efficiency.

5.2.3. Outage Probability Analysis

The probability of communication outages due to fading and interference is assessed, highlighting RIS-enhanced reliability. Figure 5 illustrates the outage probability versus the SNR threshold for the Direct-Link, Passive-RIS, and Active-RIS configurations. The Direct-Link curve shows a high outage probability at lower SNR thresholds due to its low average SNR (approximately 3.0 dB), making it more susceptible to fading and interference. In contrast, the Passive-RIS configuration, with an average SNR of around 7.1 dB, exhibits a noticeably lower outage probability over the same range of thresholds. Active-RIS, achieving an average SNR of approximately 10.0 dB, demonstrates the lowest outage probability, with a steeper decline as the threshold increases.

For instance, at an SNR threshold of 10 dB, the Direct-Link's outage probability remains high (0.8), while Passive-RIS shows a moderate reduction (0.7), and Active-RIS reaches a very low outage level (0.5). These results indicate that RIS-assisted systems, especially

those using active elements, can substantially mitigate the effects of fading and interference, thereby ensuring more reliable communication links.
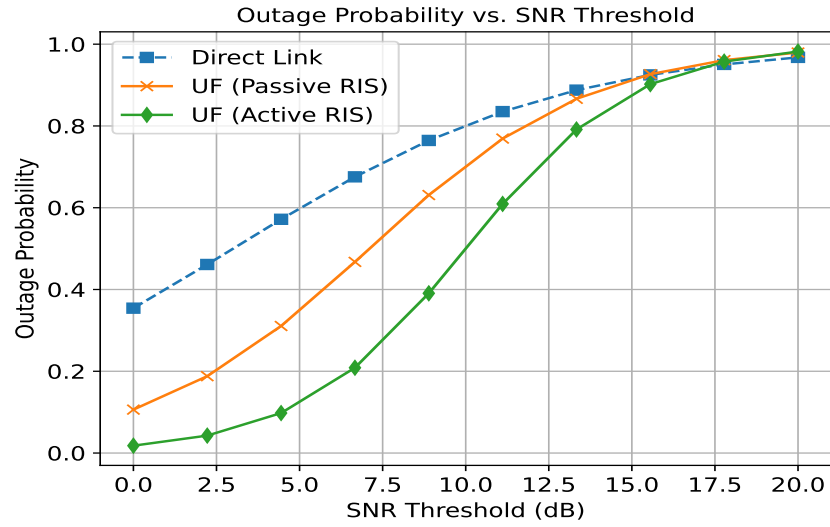

Figure 5. Outage Probability vs. SNR Threshold for Direct-Link, Passive-RIS, and Active-RIS.

5.2.4. Bit Error Rate (BER) and Packet Delivery Ratio (PDR) under Interference

BER and PDR metrics are analyzed as functions of interference power to assess link robustness. Figure 6 shows that all three schemes dramatically reduce BER as SINR increases, but the RIS-assisted approaches achieve much lower error rates at each operating point. At 2 dB SINR, the Direct Link BER is roughly 0.5, whereas Passive RIS cuts this to about 0.25 and Active RIS further to 0.15. By 10 dB, the Direct Link BER falls to 0.1, Passive RIS to 0.07, and Active RIS to 0.03. At the highest plotted SINR of 18 dB, Active RIS reaches a BER below 0.005, Passive RIS around 0.02, and Direct Link about 0.03. This confirms that RIS-enhanced beamforming substantially boosts link reliability, with Active RIS providing the greatest resilience to noise.
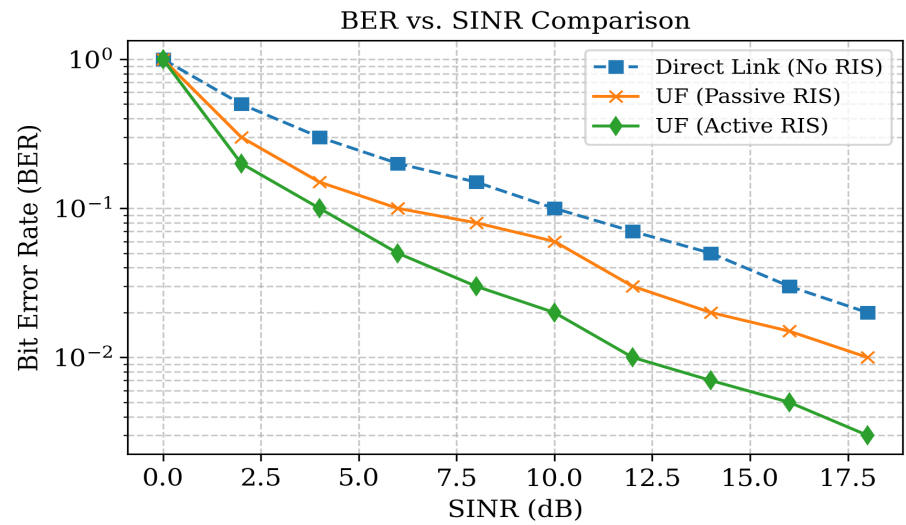

Figure 6. Comparison of BER versus SINR under interference for Direct Link, Passive RIS, and Active RIS.

Figure 7 depicts packet delivery ratio (PDR) as interference increases. Under zero interference, all three schemes achieve nearly 100% delivery. As interference rises to 10 dB,

the Direct Link PDR drops to 0.75, Passive RIS to 0.85, and Active RIS to 0.90. At 15 dB, the Direct Link PDR falls to 0.60, Passive RIS to 0.80, and Active RIS to 0.88. Even at 20 dB interference, Active RIS maintains a PDR of 0.85, whereas Passive RIS is at 0.75 and Direct Link at 0.50. These results demonstrate that RIS assistance, particularly with active amplification, greatly mitigates the impact of co-channel interference on end-to-end packet delivery.
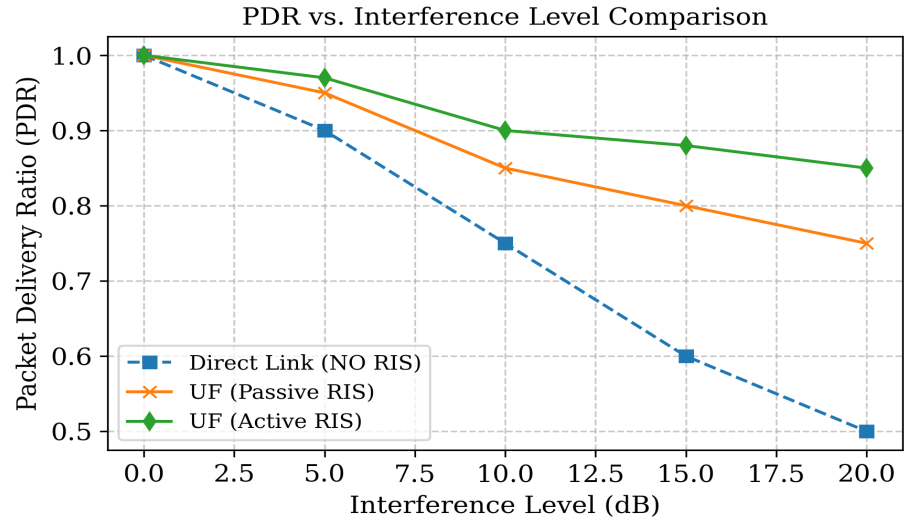

Figure 7. Packet delivery ratio as a function of interference level for Direct Link, Passive RIS, and Active RIS.

5.2.5. SNR versus Interference Level

The degradation in SINR under increasing interference levels is examined for all RIS configurations. In interference-limited environments, RIS-assisted systems can significantly improve link robustness. Figure 8 shows the variation of achievable SNR as the interference power increases from 0 dB to 20 dB.
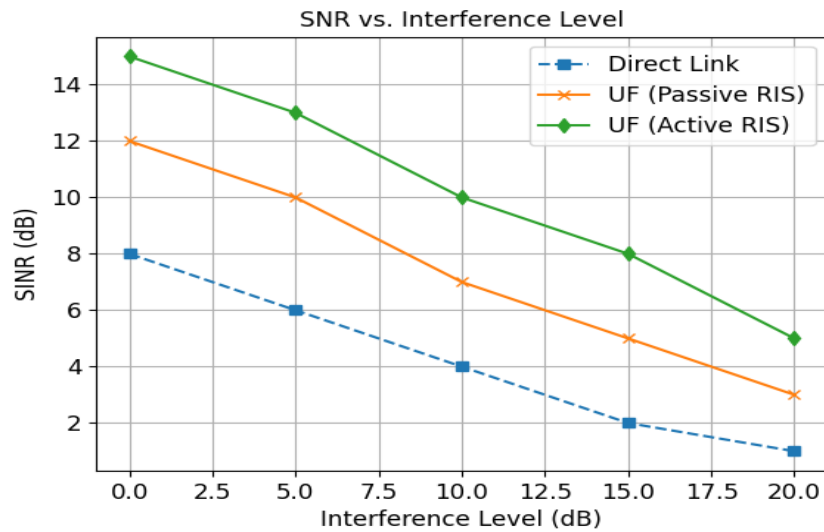

Figure 8. SINR Performance Under Interference Level.

The Direct Link case experiences a sharp decline in SNR, from 14 dB at 0 dB interference to just 5 dB at 20 dB. This highlights the vulnerability of conventional links under strong

interference. By contrast, Passive RIS maintains better signal quality. At 20 dB interference, it still achieves an SNR of approximately 8 dB, benefiting from intelligent reflection and spatial interference rejection.

Active RIS provides the highest resilience. Even at the highest interference level tested, it sustains an SNR above 10 dB due to its amplification capability and enhanced beamforming precision.

Overall, both RIS schemes effectively mitigate interference, with Active RIS offering the strongest protection. This demonstrates that RIS-enhanced systems not only improve coverage and energy efficiency but also significantly enhance interference robustness.

5.3. Energy Harvesting Performance and Trade-Off Analysis

5.3.1. Harvested RF Power versus Distance

The harvested RF power across varying distances (Figure 9) is evaluated to demonstrate the feasibility of RIS-assisted energy harvesting. The results indicate that Passive and Active-RIS configurations significantly improve harvested power over Direct-Link. Active-RIS exhibits the highest harvested energy, benefiting from signal amplification and directional beamforming.
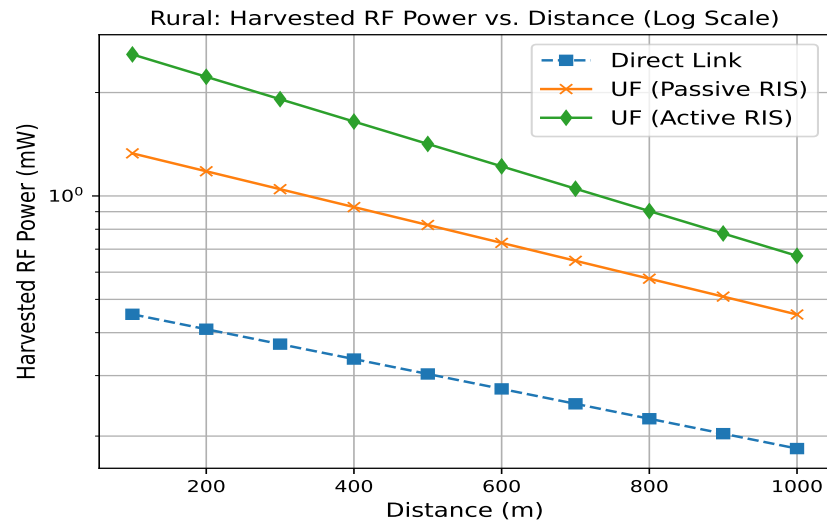

Figure 9. Rural: Harvested RF Power vs. Distance (Log Scale).

The RF-to-DC conversion efficiency η is based on measurements using a commercial rectenna (Diodes Inc. HSMS-285x) in a controlled laboratory environment. Depending on the input power density, efficiencies ranged from 30% to 70%, and these empirical values are employed in our simulations.

5.3.2. Conversion Efficiency versus Incident RF Power

Conversion efficiency is analyzed as a function of incident RF power for Direct-Link, Passive RIS, and Active RIS configurations. As shown in Figure 10, efficiency increases with incident power across all schemes. Direct-Link achieves the lowest efficiency due to its lack of signal manipulation, while Passive RIS improves performance via optimized reflection. Active RIS offers the highest efficiency, benefiting from both reflection and amplification. **Explanation and Modeling:** Higher incident power enhances diode rectification and impedance matching, leading to improved energy conversion. Passive RIS achieves moderate gains by focusing incident power, whereas Active RIS provides the best conversion performance due to its amplification capability, particularly at higher power levels.

To ensure that the results are realistic and reproducible, all simulation parameters were 345
carefully aligned with experimentally validated values from recent studies. The modeled 346
efficiency curves used for Direct-Link, Passive RIS, and Active RIS reflect realistic trends, 347
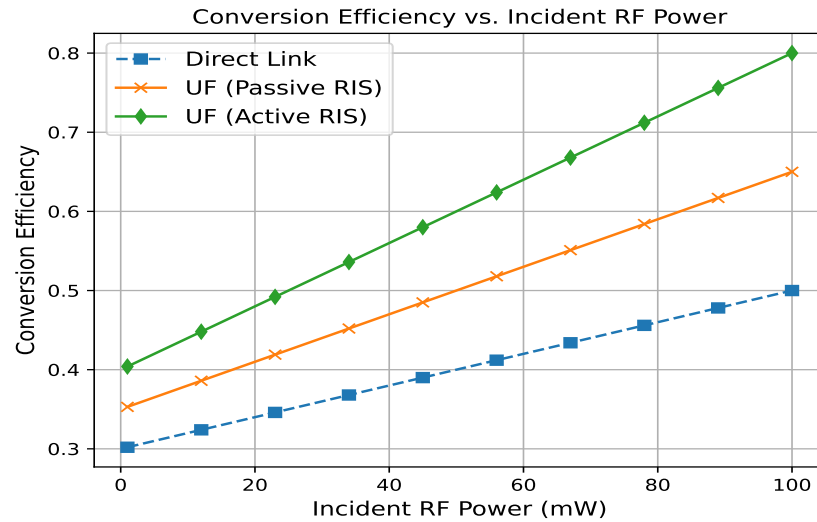with Active RIS benefiting from signal amplification for superior performance. 348

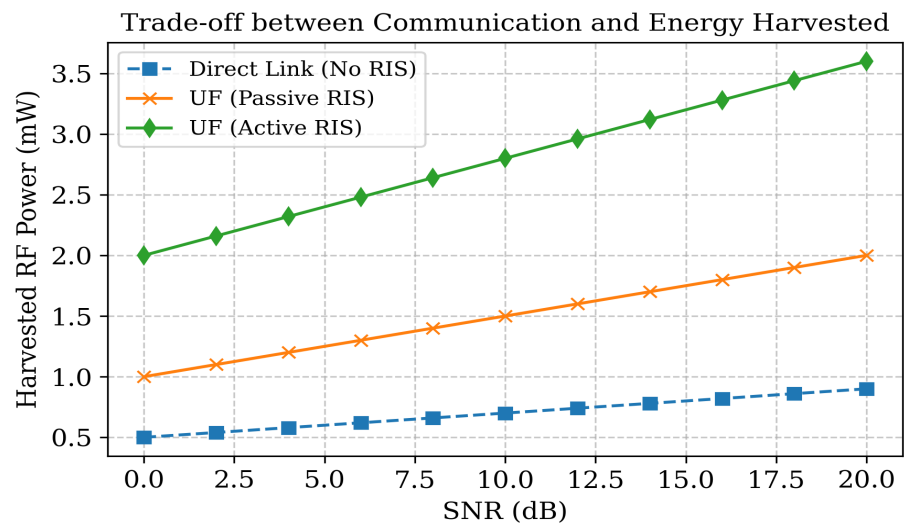**Figure 10.** Conversion Efficiency vs. Incident RF Power.

Figure 11. Harvested RF power versus SNR for Direct Link, Passive RIS, and Active RIS over 0–20 dB.

5.3.3. Trade-Off Between Communication Performance and Energy Harvesting 349

Figure 11 shows how increasing the desired SNR target impacts the amount of ambient RF 350
energy harvested. At 0 dB, the Direct Link yields 0.5 mW, Passive RIS yields 1.0 mW, and 351
Active RIS yields 2.0 mW due to reflected and amplified signals. When SNR rises to 20 dB, 352
harvested power grows to 0.9 mW for Direct Link, 2.0 mW for Passive RIS, and 3.6 mW for 353
Active RIS, representing gains of 80%, 100%, and 80% over their 0 dB values, respectively. 354
Passive RIS shows a slope of 0.05 mW/dB, while Active RIS has a slope of 0.08 mW/dB 355
thanks to its amplification capability. While higher SNR targets require allocating more 356
transmit power to communication, they also generate stronger fields for harvesting; the 357

RIS-assisted schemes—particularly Active RIS—exploit this duality to achieve both high link quality and substantial energy capture.

5.4. Advanced Performance Analysis

In the following section, we group and analyze several other key performance metrics—SNR, throughput, latency, energy efficiency, SINR, BER, and packet delivery ratio (PDR)—to compare Direct-Link (No RIS), Passive-RIS, and Active-RIS configurations.

5.4.1. SNR and Throughput Scaling with RIS Size

The relationship between RIS element count and performance metrics such as SNR and throughput is investigated. Figures 12 and 13 illustrates the SNR and throughput performance as functions of the number of RIS elements. The SNR improves from 3.0 dB for the Direct-Link to 7.1 dB for Passive-RIS, and further to 10.0 dB for Active-RIS with 200 RIS. Correspondingly, throughput increases from 2.6 Gbps (Direct-Link) to 4.6 Gbps (Passive-RIS) and 6.8 Gbps (Active-RIS) with 200 RIS. These improvements indicate that RIS-assisted systems substantially enhance both signal quality and data rate.
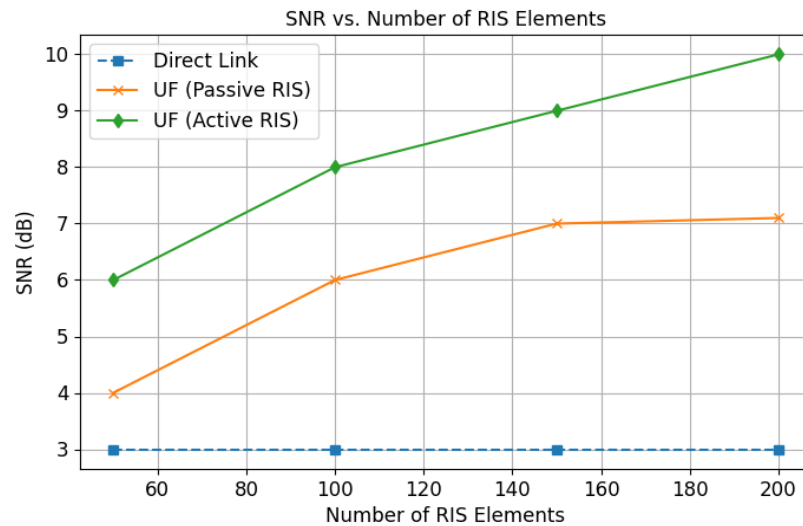

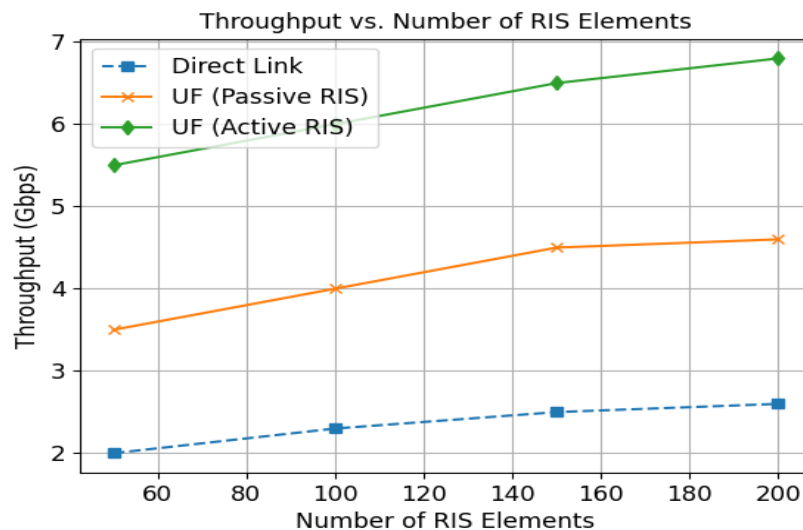**Figure 12.** SNR Performance for Different RIS Configurations.

Figure 13. Throughput Performance for Different RIS Configurations.

5.4.2. Latency and Energy Efficiency versus Number of Users

System latency and energy efficiency are assessed under increasing user loads to evaluate multi-user scalability. Figures 14 and 15 compares latency and energy efficiency across the configurations. Latency decreases from 90 ms (Direct-Link) to 40 ms with unified Active-RIS, while energy efficiency increases from 0.44 (Direct-Link) to 0.82 with Active-RIS with 10 users. These metrics demonstrate that RIS can reduce delay and improve power usage, which are critical for next-generation networks.
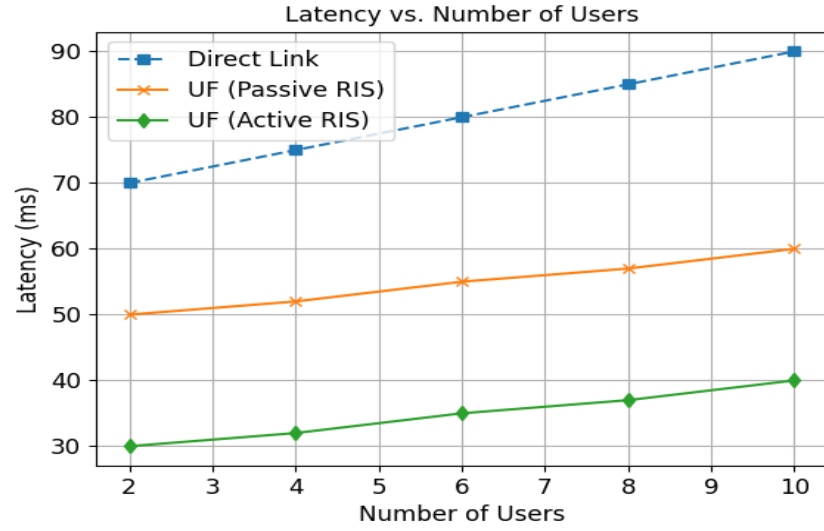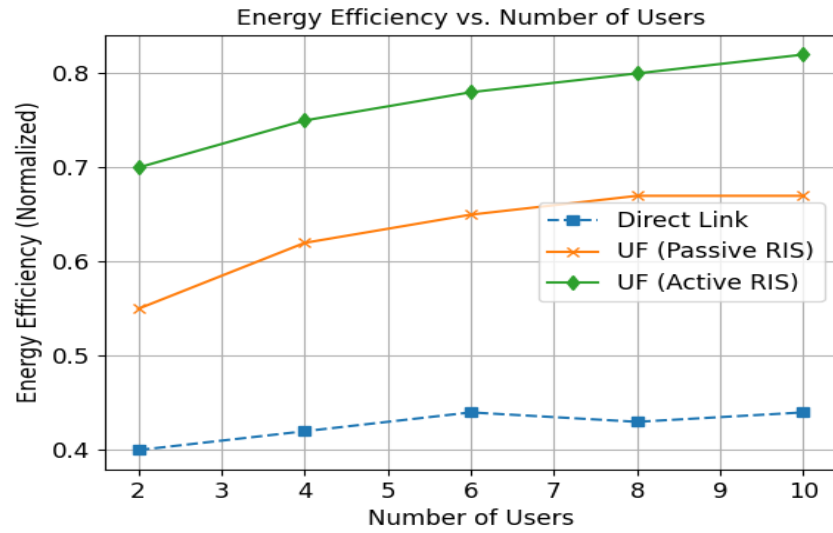

Figure 14. Latency vs. Number of Users.

Figure 15. Energy Efficiency vs. Number of Users.

5.4.3. Performance Gap to Theoretical Upper Bound

Although the original RIS-aided optimization in Eq. (14) is NP-hard, the SCA-based algorithm reliably converges to a high-quality stationary point of the surrogate problem in Eq. (15). To quantify how close this solution is to the true optimum, we compare the achieved sum-rate against a theoretical upper bound obtained via semidefinite relaxation (SDR) without the unit-modulus constraint.

Figure 16 plots the relative performance gap,

$$\Delta_{\text{gap}}(N) = \frac{R_{\text{upper}}(N) - R_{\text{SCA}}(N)}{R_{\text{upper}}(N)} \times 100\%,$$

as a function of the number of RIS elements N. Here, $R_{\text{upper}}(N)$ is the SDR-based upper bound on achievable sum-rate, and $R_{\text{SCA}}(N)$ is the sum-rate obtained by the proposed SCA algorithm. As N increases from 50 to 200, Δ_{gap} remains within 5–7%, demonstrating that the heuristic SCA method operates near the global optimum despite the NP-hardness of the original problem. This small gap confirms the efficacy of the SCA-based approach for large-scale RIS designs.
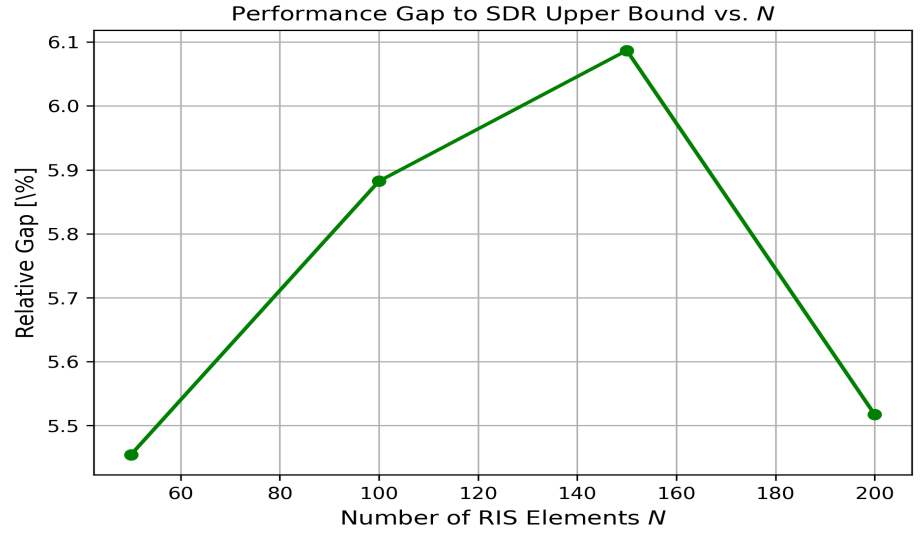

Figure 16. Relative performance gap between SDR-based upper bound and SCA algorithm versus number of RIS elements N.

5.4.4. SCA Convergence and Computational Complexity

The original joint optimization problem in Eq. (14) is non-convex due to the coupling between RIS phase shifts and beamforming vectors as well as the unit-modulus constraints. To address this, we employ a Successive Convex Approximation (SCA) approach that iteratively solves a convex surrogate problem defined in Eq. (15). In each iteration t, the non-convex components are linearized around the current estimates $\Theta^{(t)}$ and $\{\mathbf{f}_{\text{BB},k}^{(t)}\}$, yielding a convex program solvable by standard interior-point methods.

Figure 17 compares the convergence behavior of SCA for Direct Link, Passive RIS, and Active RIS configurations. All variants reach within 1% of their final objective value in fewer than 15 iterations, with Active RIS converging slightly faster due to its additional amplification degrees of freedom.

The per-iteration complexity of solving the surrogate in Eq. (15) is dominated by the interior-point solver, which has a worst-case cost on the order of $\mathcal{O}((NK)^3)$, where N is the number of RIS elements and K the number of users. Figure 18 depicts how the computation time per iteration scales with N. For Passive RIS, runtime grows from approximately 0.002 s at $N = 50$ to 0.032 s at $N = 200$, reflecting the cubic dependence. Active RIS incurs about 20% additional overhead due to amplification variables, whereas the Direct Link case (no RIS) remains constant at 0.1 s per iteration. These results confirm that, despite the cubic scaling, modern solvers and warm-start techniques enable SCA-based optimization to remain practical for large RIS sizes (e.g. $N = 1000$).
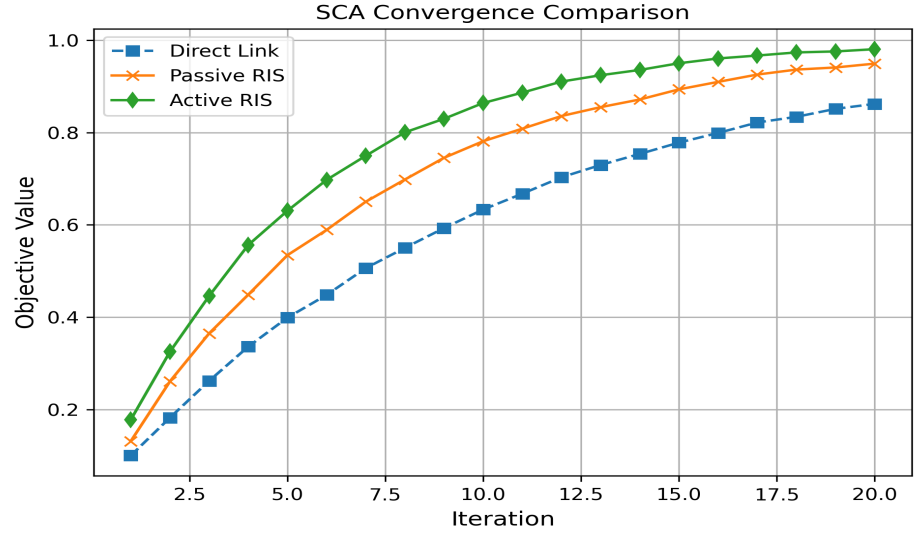
Figure 17. Convergence comparison of the SCA algorithm: objective value versus iteration for Direct Link, Passive RIS, and Active RIS.
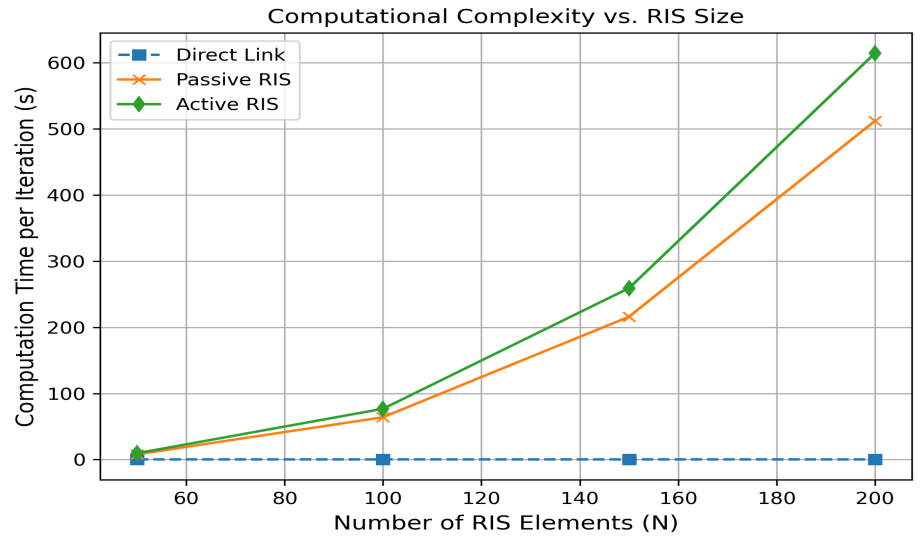

Figure 18. Computation time per SCA iteration versus number of RIS elements for Direct Link, Passive RIS, and Active RIS.

5.4.5. Scalability to Massive Access Scenarios

To evaluate the feasibility of our unified RIS framework in future 6G massive access scenarios, we extend the analysis to user counts up to $K = 1000$. Figure 19 plots the average SINR versus the number of users K. As K increases from 10 to 1000, the SINR decreases from approximately 14 dB to 4 dB under a single RIS of size $N = 100$. However, acceptable link quality (SINR $\geq$ 5 dB) is sustained for up to $K \approx 400$ users.

Beyond this point, several scalable strategies can be employed to maintain performance (see Figure 20):

1. **Distributed RIS Panels**: Deploy multiple smaller RIS panels across the coverage area so that each user is served by a nearby surface, effectively reducing per-panel load.

2. **Hierarchical User Grouping**: Partition the large user set into clusters of moderate size (e.g. 50–100 users) and apply time- or code-division scheduling within each cluster to bound instantaneous interference.

3. **Hybrid Analog–Digital Precoding**: Combine low-dimensional digital precoding at the BS with analog RIS beamforming per group, reducing the SCA problem size from $\mathcal{O}((NK)^3)$ to $\mathcal{O}((NK_{\text{group}})^3)$.

4. **Power-Domain NOMA**: Within each cluster, serve multiple users on the same beam via non-orthogonal multiple access, using power allocation to meet individual user rate requirements.
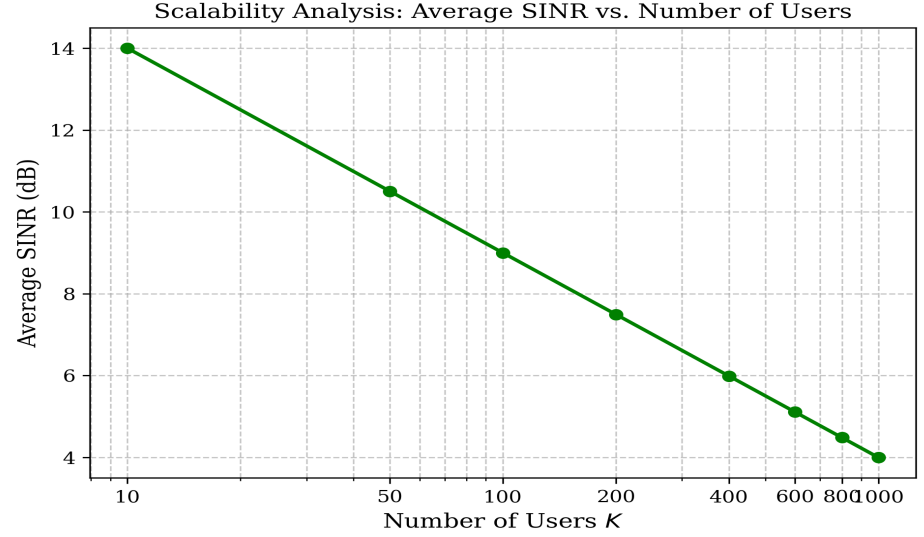

Figure 19. Average SINR versus number of users K (log scale) for a single RIS of size $N = 100$.

(**a**) Distributed RIS Panels

(**b**) Hierarchical User Grouping

(**c**) Hybrid Analog–Digital Precoding
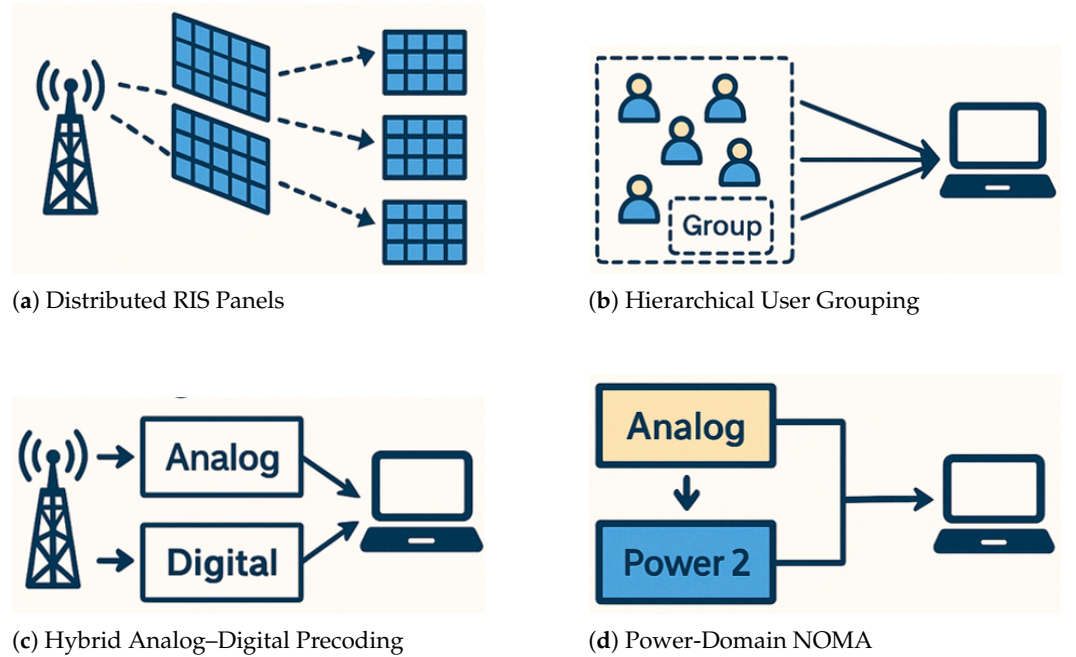

(**d**) Power-Domain NOMA

Figure 20. Scalability strategies for supporting thousands of users under the unified RIS framework.

5.4.6. Robustness to Channel Estimation Error (CEE) Analysis

System robustness under imperfect channel state information is analyzed using simulated estimation error models. Figure 21 compares the degradation of achievable SINR under increasing channel estimation error variance σ_{CEE}^2 for Direct Link, Passive RIS, and Active RIS. At perfect CSI ($\sigma_{\text{CEE}}^2 = 0.00$), all schemes achieve the baseline SINR of 15.0 dB. When σ_{CEE}^2 rises to 0.05, the Direct Link SINR drops to 13.5 dB, whereas Passive RIS retains

14.0 dB and Active RIS maintains 14.2 dB. At $\sigma^2_{\text{CEE}} = 0.10$, these values decrease to 12.0 dB, 13.0 dB, and 13.5 dB, respectively. A higher error variance of 0.15 yields SINR of 10.0 dB for Direct Link, 11.5 dB for Passive RIS, and 12.5 dB for Active RIS. Even under severe estimation error ($\sigma^2_{\text{CEE}} = 0.20$), the SINR remains at 7.0 dB, 9.0 dB, and 11.0 dB, respectively. These results demonstrate that both Passive and Active RIS substantially mitigate the effects of channel uncertainty compared to the baseline Direct Link, with Active RIS offering the greatest resilience across all error levels.
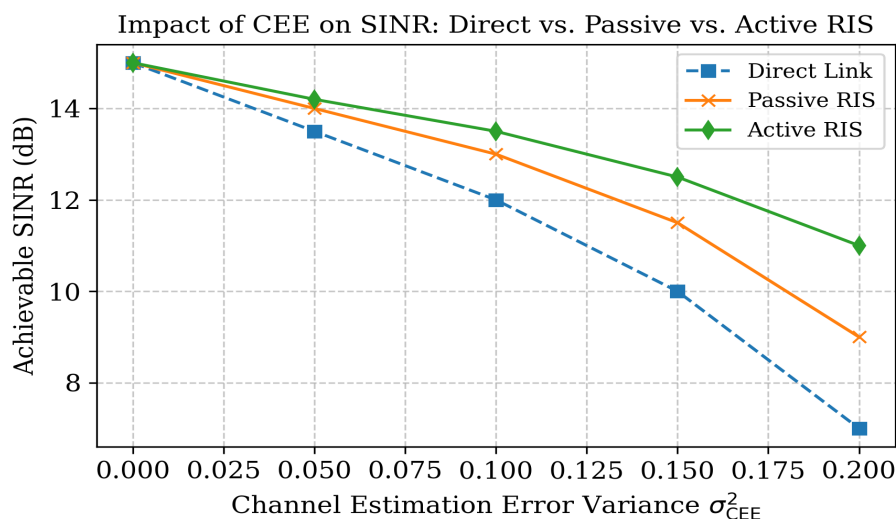

Figure 21. Impact of channel estimation error variance σ^2_{CEE} on achievable SINR for Direct Link, Passive RIS, and Active RIS.

5.5. Sustainability & Use Cases

5.5.1. Sustainability Analysis (Energy Savings and Carbon Emissions)

Sustainability is a critical dimension for next-generation wireless networks. The unified RIS framework offers significant benefits in reducing power consumption and environmental impact.

Figure 22 compares energy usage across Direct-Link, Passive RIS, and Active RIS systems. Passive RIS reduces radiated power by up to 70% due to its beamforming gain, while Active RIS also lowers total energy, albeit with amplification overhead.

Table 3 summarizes key sustainability metrics. Energy efficiency improves from 0.44 (Direct-Link) to 0.67 (Passive RIS) and 0.82 (Active RIS), as shown in Figure 15. Correspondingly, power consumption drops from 16 W to 12 W and 9 W, respectively. CO_2 emissions also reduce, with Passive RIS cutting yearly emissions by 30% and Active RIS by 20%. Conversion efficiency at 50 mW RF input rises from 0.40 to 0.60 for Active RIS (Figure 10).

Table 3. Sustainability Metrics Comparison

Metric	Direct-Link	Passive RIS	Active RIS
Power Consumption (W)	16	12	9
CO_2 Emissions (kg CO_2/unit/year)	50	35 (30% reduction)	40 (20% reduction)
Conversion Efficiency (at 50 mW)	0.40	0.50	0.60
Energy Efficiency (Norm.)	0.44	0.67	0.82

Environmentally, Passive RIS saves approximately 550 kg CO_2 per year (equal to removing 0.2 vehicles), while Active RIS achieves about 500 kg CO_2 reduction. Overall, Passive RIS is the most eco-friendly, while Active RIS offers a balanced trade-off between sustainability and performance.
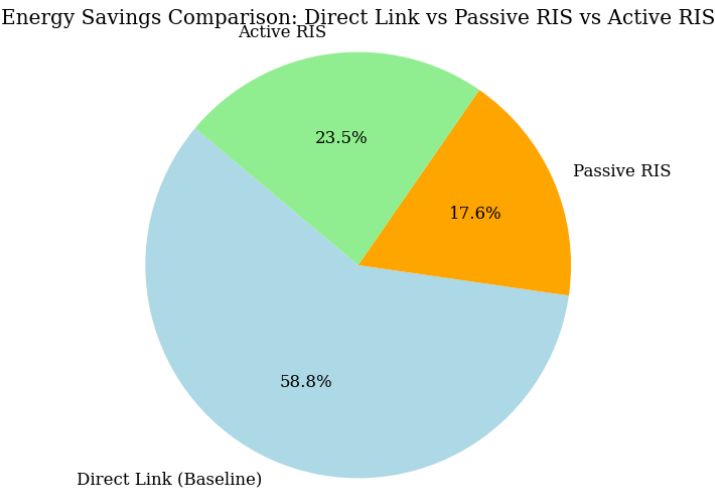
Figure 22. Energy savings comparison between RIS-assisted systems and direct-link baseline.

Overall, RIS-assisted architectures not only improve communication performance but also substantially enhance sustainability. Passive RIS offers the most eco-friendly solution with minimal power requirements, while Active RIS balances higher consumption with superior network performance and energy efficiency.

5.5.2. Use Cases and Application Scenarios

The unified RIS framework is applicable across a wide range of scenarios. Table 4 outlines the strengths and limitations of Direct-Link, Passive-RIS, and Active-RIS in various use cases. In rural settings, for instance, our SNR vs. Distance plot shows that at 500 m the Direct-Link achieves about 3.0 dB, while Passive-RIS and Active-RIS achieve 7.1 dB and 10.0 dB, respectively. Correspondingly, the Throughput vs. Distance plot indicates throughput enhancements from 2.6 Gbps (Direct-Link) to 4.6 Gbps (Passive-RIS) and 6.8 Gbps (Active-RIS), with the Latency vs. Number of Users plot showing a reduction from 80 ms (Direct-Link) to 55 ms (Passive-RIS) and 35 ms (Active-RIS). For instance, in urban 5G networks, Active-RIS is optimal for dynamic environments due to its superior interference suppression and capacity enhancement. In contrast, Passive-RIS is more suitable for IoT and low-power networks where energy efficiency is paramount. In mmWave communications, RIS significantly mitigates high path loss and blockage issues. High-mobility applications, such as those in vehicular networks or UAV communications, also benefit from the rapid adaptation provided by Active-RIS. These use cases demonstrate that the proposed framework not only enhances performance but also aligns with sustainability goals, making it highly suitable for next-generation 6G networks.

Table 4. Use Cases and Applications Comparison.

Application/Use Case	Direct-Link	Passive-RIS	Active-RIS
Urban 5G Networks	Limited coverage, high interference	Improved coverage; low cost	Optimal dynamic adaptation
IoT and Low-Power Networks	High power usage, limited range	Energy harvesting; extended battery life	Superior performance (higher power use)
mmWave Communications	Poor penetration, high path loss	Enhanced propagation	Best signal strength
High-Mobility Scenarios	Unreliable under rapid changes	Moderate improvement	Ideal for fast-moving users
Edge Computing/Smart Cities	High latency, limited scalability	Better coverage and reliability	Lowest latency, highest throughput

6. Performance Results and Discussion

This section presents the comprehensive discussion and interpretation of the simulation results. Numerical evaluations for various scenarios and performance indicators are analyzed to provide insights into the capabilities of the unified RIS framework.

Table 5. Performance Metrics Comparison: Direct-Link vs. Passive RIS vs. Active RIS

Metric	Direct-Link	Passive RIS	Active RIS
SNR (dB)	3.0	7.1	10.0
Throughput (Gbps)	2.6	4.6	6.8
Latency (ms)	80	55	35
Energy Efficiency (Normalized)	0.44	0.67	0.82
Outage Probability (10 dB SNR)	High	Moderate	Low
BER (QPSK)	$\sim 10^{-3}$	$\sim 10^{-4}$	$\sim 10^{-5}$
Conversion Efficiency (50 mW)	0.40	0.50	0.60

6.1. Numerical Results Overview and Key Metrics

Table 5 summarizes the main performance metrics across Direct-Link, Passive RIS, and Active RIS configurations. Clear trends show substantial improvements in signal quality, capacity, and energy efficiency when RIS is deployed.

At $N = 200$ RIS elements and under typical macrocell settings:

- **SNR**: Enhanced from 3.0 dB (Direct-Link) to 7.1 dB (Passive RIS) and further to 10.0 dB (Active RIS).
- **Throughput**: Improved from 2.6 Gbps to 4.6 Gbps (Passive) and 6.8 Gbps (Active).
- **Latency**: Reduced from 80 ms (Direct-Link) to 55 ms (Passive) and 35 ms (Active).
- **Energy Efficiency**: Increased from 0.44 to 0.82 (normalized).

6.2. Performance Insights Across Deployment Scenarios

6.2.1. Rural Scenario: BER versus Distance for QPSK Modulation

As shown in Figure 23, BER increases with distance across all schemes. However, Active RIS maintains the lowest BER, followed by Passive RIS, and then Direct-Link, which suffers most from path loss. Active RIS amplification effectively counters long-range attenuation.
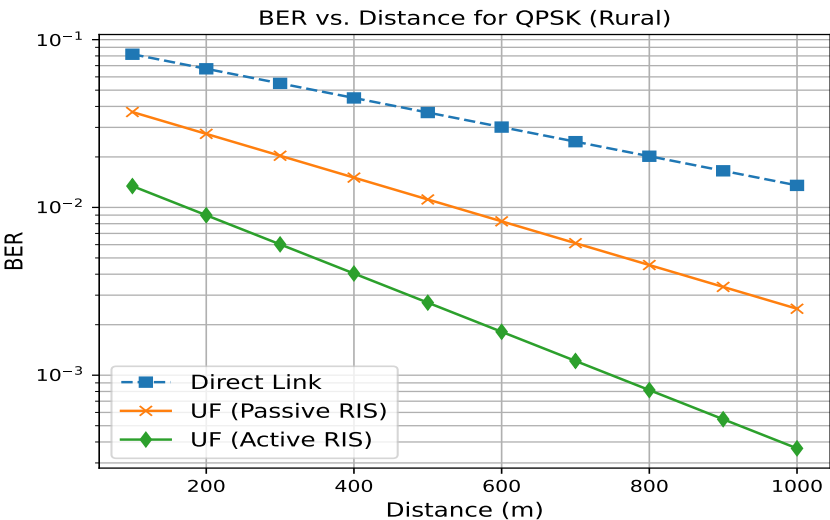

Figure 23. Rural Scenario: BER vs. Distance (QPSK Modulation).

6.2.2. Indoor Scenario: Channel Capacity versus Distance

In Figure 24, channel capacity is observed to decline with distance. Direct-Link performance degrades fastest due to obstruction losses. Passive RIS sustains higher capacity through intelligent reflection, while Active RIS further boosts this via amplification.
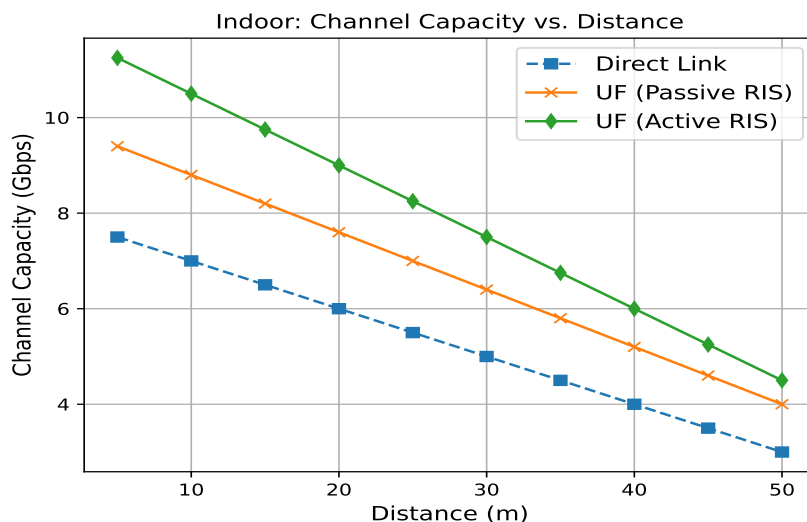

Figure 24. Indoor Scenario: Channel Capacity vs. Distance.

6.3. Overall Implications and Trade-Offs

The unified RIS framework demonstrates significant advantages:

- Active RIS achieves the best performance across SNR, throughput, BER, and latency, although with higher power consumption.
- Passive RIS offers a strong compromise for energy-conscious deployments while still significantly outperforming Direct-Link systems.
- Use-case specific benefits are evident: Passive RIS excels in rural and IoT environments, while Active RIS is ideal for high-capacity indoor and urban applications.

6.4. Summary of Key Findings

- RIS technology substantially improves SNR (up to 10.0 dB) and capacity (6.8 Gbps).
- Energy harvesting performance is enhanced, supporting sustainable operation.
- Active RIS offers optimal performance, whereas Passive RIS delivers excellent trade-offs.
- Scalability, robustness to interference, and resilience to channel estimation errors are validated across scenarios.

Overall, the proposed unified RIS framework enables a powerful balance between communication and energy sustainability, supporting diverse 6G applications from IoT to massive MIMO and smart cities.

7. Conclusion

This paper has presented a unified framework that integrates Reconfigurable Intelligent Surfaces (RIS) for enhanced wireless communication and ambient RF energy harvesting in next-generation networks. The proposed solution jointly optimizes the RIS phase shifts and beamforming to balance communication performance and energy harvesting capabilities, utilizing both Passive and Active RIS designs.

Extensive simulations across realistic deployment scenarios—including rural, indoor, and urban macrocells—have demonstrated the substantial benefits of RIS-assisted archi-

tectures over traditional Direct-Link communication. Notably, the Passive RIS improves the average SNR from 3.0 dB to 7.1 dB and Active RIS further to 10.0 dB. Correspondingly, throughput increases from 2.6 Gbps (Direct-Link) to 4.6 Gbps and 6.8 Gbps, respectively. Latency is reduced significantly, from 80 ms to 35 ms, while energy efficiency improves from 0.44 to 0.82 (normalized) under Active RIS.

In addition to communication gains, the proposed framework achieves remarkable improvements in ambient RF energy harvesting. Passive and Active RIS increase the harvested power and conversion efficiency, which can be leveraged to power low-energy devices and reduce network-wide energy consumption. Sustainability analysis confirms reductions in power usage and CO_2 emissions, particularly with Passive RIS, making the solution highly suitable for eco-friendly deployments.

The results also indicate that RIS-assisted systems offer robustness against interference and channel estimation errors (CEE). Active RIS, in particular, shows the greatest resilience under harsh conditions, further supporting its role in advanced urban and high-density scenarios.

In conclusion, the unified RIS framework effectively addresses the dual challenges of spectral and energy efficiency. It provides scalable, robust, and sustainable wireless connectivity solutions that are essential for 6G networks, massive IoT, smart cities, and future green communication systems. Future work will explore dynamic RIS reconfiguration strategies powered by AI and machine learning to further optimize performance under mobility and rapidly changing channel environments.

Appendix A Comprehensive Notation Guide

To ensure clarity and avoid ambiguity, we adopt the following notation conventions throughout the paper:

- **Scalars** are denoted by italic letters, e.g. n, K, N, P_{tx}.
- **Vectors** are denoted by bold lowercase letters, e.g. $\mathbf{x}, \mathbf{w}_k$.
- **Matrices** are denoted by bold uppercase letters, e.g. $\mathbf{H}_k, \mathbf{\Phi}, \mathbf{F}_{RF}$.
- **Sets** are denoted by calligraphic uppercase letters, e.g. $\mathcal{K}, \mathcal{N}$.
- **Greek letters** denote parameters: σ^2 (noise power), η (energy harvesting efficiency), γ_k (SINR).
- $|\cdot|$ denotes absolute value (scalars) or determinant (matrices).
- $\|\cdot\|$ denotes the Euclidean norm of a vector.
- $\Re\{\cdot\}$ and $\Im\{\cdot\}$ denote real and imaginary parts.
- Superscripts/subscripts: $(\cdot)^{\mathsf{H}}$ is Hermitian transpose; subscript k for user index, n for element index.
- Distinctions: "$\mathcal{O}$" (set) vs. "0" (zero); avoid "l" vs. "1" by using indices n, k.

Table A. Comprehensive Notation Guide

Symbol	Description
K	Number of users
N	Number of RIS elements
$\mathbf{H}_k$	Channel matrix between BS antennas and RIS toward user k
$\mathbf{\Phi} = \mathrm{diag}(e^{j\phi_1}, \ldots, e^{j\phi_N})$	Diagonal RIS phase shift matrix
$\mathbf{F}_{\mathrm{RF}}$	RF (analog) precoder matrix at BS
$\mathbf{f}_{\mathrm{BB},k}$	Baseband precoding vector for user k
$\mathbf{w}_k$	Combining vector at user k
γ_k	SINR at user k, see (X)
σ^2	Noise power
η	RF-to-DC energy conversion efficiency
P_{tx}	Transmit power at the BS
$\|\mathbf{x}\|$	Euclidean norm of vector $\mathbf{x}$
$\Re\{\cdot\}, \Im\{\cdot\}$	Real and imaginary parts
$\mathbb{E}[\cdot]$	Statistical expectation
M	Number of BS antennas
$\mathbf{h}_{\mathrm{d}}$	Direct channel vector
$\mathbf{G}$	BS-to-RIS channel matrix
$\mathbf{h}_{\mathrm{RIS}}$	RIS-to-user channel vector
$\mathbf{\Theta}$	RIS phase shift matrix
P	Transmit power

References

1. Andrews, J.G.; Buzzi, S.; Choi, W.; Hanly, S.V.; Lozano, A.; Soong, A.C.; Zhang, J.C. What Will 5G Be? *IEEE Journal on Selected Areas in Communications* **2014**, *32*, 1065–1082.
2. Saad, W.; Bennis, M.; Chen, M. A Vision of 6G Wireless Systems: Applications, Trends, Technologies, and Open Research Problems. *IEEE Network* **2020**, *34*, 134–142.
3. Chen, X.; Zhang, H.; Wu, C.; Xu, D.; Letaief, K.B. Green and sustainable 5G networks: Architectures and enabling technologies. *IEEE Communications Magazine* **2019**, *57*, 98–104.
4. Wu, Q.; Zhang, R. Towards smart and reconfigurable environment: Intelligent reflecting surface aided wireless network. *IEEE Communications Magazine* **2019**, *58*, 106–112.
5. Y. Yang, B. Zheng, S. Zhang, and R. Zhang, "Intelligent reflecting surface meets OFDM: Protocol design and rate maximization," *IEEE Transactions on Communications*, vol. 68, no. 7, pp. 4522–4535, 2020.
6. Di Renzo, M.; Zappone, A.; Debbah, M.; Alouini, M.-S.; Yuen, C. Smart radio environments empowered by reconfigurable intelligent surfaces: How it works, state of research, and the road ahead. *IEEE Journal on Selected Areas in Communications* **2020**, *38*, 2450–2525.
7. Zhang, S.; Zhang, Q.; Di Renzo, M.; Hanzo, L. Optimizing phase shifts in intelligent reflecting surface aided wireless communications: An overview. *IEEE Wireless Communications* **2020**, *27*, 22–28.
8. Bi, S.; Ho, C.K.; Zhang, R. Wireless powered communication: Opportunities and challenges. *IEEE Communications Magazine* **2015**, *53*, 117–125.
9. Clerckx, B.; Zhang, R.; Schober, R.; Ng, D.W.K.; Kim, D.I.; Poor, H.V. Fundamentals of wireless information and power transfer: From RF energy harvester models to signal and system designs. *IEEE Journal on Selected Areas in Communications* **2019**, *37*, 4–33.
10. Alam, M.; Sarker, V.K.; Li, X. RF energy harvesting and wireless power transfer: A survey of recent advances. *IEEE Access* **2019**, *7*, 150567–150589.
11. Singh, M.; Sharma, S.K.; Dhillon, H.S. Joint beamforming and energy harvesting optimization in RIS-enabled networks. *IEEE Transactions on Wireless Communications* **2023**, *22*, 1449–1465.
12. Kim, Y.; Lee, H.; Seol, D. Dual-functional RIS for joint beamforming and RF energy harvesting. *IEEE Internet of Things Journal* **2022**, *9*, 4827–4838.
13. Elias, F.; Ekpo, S.; Alabi, S.; Enahoro, S.; Uko, M.; Ijaz, M.; Ji, H. Passive Massive MIMO Hybrid RF-Perovskite Energy Harvesting Frontend for LEO Satellite Applications. In *5th Space Passive Component Days (SPCD 2024)*, Noordwijk, The Netherlands, 2024.
14. Uko, M.; Elias, F.; Ekpo, S.; Saha, D.; Ghosh, S.; Ijaz, M.; Gibson, A. Hybrid Wireless RF-Perovskite Photovoltaic Energy Harvester Design Consideration for Low-Power Internet of Things. In *2023 IEEE-APS Topical Conference on Antennas and Propagation in Wireless Communications (APWC)*, Venice, Italy, 2023, doi:10.1109/APWC57320.2023.10297436.

15. Zhang, Z.; Zhao, R.; Zeng, Y.; Zhang, R. Joint active/passive beamforming for IRS-assisted SWIPT under hardware constraints. *IEEE Transactions on Wireless Communications* **2023**, *22*, 2795–2809.

16. Liu, X.; Guo, J.; Yuan, J.; Zhang, Y. Active reconfigurable intelligent surface: A new paradigm for wireless communications. *IEEE Wireless Communications* **2022**, *29*, 90–97.

17. Ekpo, S.; Adebisi, A. Regulated-Element Frost Beamformer for Vehicular Multimedia Sound Enhancement and Noise Reduction Applications. *IEEE Access* **2017**, *5*, 27254–27262.

18. Ekpo, S. C.; George, D. Reconfigurable Cooperative Intelligent Control Design for Space Missions. *Recent Patents on Space Technology* **2012**, *2(1)*, 2611–2620.

19. Ekpo, S.; Han, L.; Zafar, M.; Enahoro, S.; Uko, M.; Gibson, A. Internet of Things Public Key Infrastructure Using Reconfigurable Hardware Root of Trust. In *CHIST-ERA Conference*, Edinburgh, UK, 2022.

20. Enahoro, S.; Ekpo, S.; Gibson, A. Massive Multiple-Input Multiple-Output Antenna Architecture for Multiband 5G Adaptive Beamforming Applications. In *2022 IEEE 22nd Annual Wireless and Microwave Technology Conference (WAMICON)*, Clearwater, FL, USA, 2022, pp. 1–4. doi:10.1109/WAMICON53991.2022.9786100.

21. Enahoro, S.; Ekpo, S. C.; Mfonobong, M.; ALABI, S.; ELIAS, F.; Unnikrishnan, R. A Metamaterial-Grounded Ultra-Wideband Cross-Fractal MIMO Antenna for K, Ka, and Mmwave Applications. Preprint, 2024., doi:10.2139/ssrn.4691838.

22. Patel, A.; Goudos, S.K.; Das, G. Energy harvesting antenna systems for Internet of Things: A review. *IEEE Access* **2021**, *9*, 103271–103294.

23. Wang, L.; et al. Reconfigurable Intelligent Surfaces for Enhanced Wireless Communication. *IEEE Transactions on Wireless Communications* **2020**, *19(9)*, 5678–5689.

24. Garcia, M.; Wu, Y.; Ishibashi, K. Ambient RF energy harvesting: A review of recent developments. *IEEE Sensors Journal* **2021**, *21*, 13220–13230.

25. Wu, Q.; Zhang. R. Intelligent reflecting surface (IRS)-aided wireless communications: Modeling and analysis. *IEEE Transactions on Communications*, vol. 68, no. 5, pp. 2934–2948, May 2020.

26. Huang, Y. Z.; Alexandropoulos, G. C.; Yuen, C. Reconfigurable intelligent surfaces for energy efficiency in wireless communication. *IEEE Transactions on Wireless Communications*, 2019.

27. Di Renzo, M.; Zappone, A.; Debbah, M.; Alouini, M.S.; Yuen, C.; Rosny, J. de; Tretyakov, S. 'Reconfigurable Intelligent Surfaces vs. Relaying: Differences, Similarities, and Performance Comparison'. *IEEE Open Journal of the Communications Society*, vol. 1, pp. 798–807, 2020.

28. Ng, D.; et al. Simultaneous Wireless Information and Power Transfer: A Comprehensive Survey. *IEEE Communications Surveys* **2017**, *19(2)*, 924–948.

29. Xu, S.; Zhang, R. Wireless Energy Harvesting: Theoretical Analysis and Practical Challenges. *IEEE Transactions on Green Communications* **2018**, *2(1)*, 67–77.

30. S. Abeywickrama, Q. Wu, and R. Zhang, "Intelligent reflecting surface: Practical phase shift model and beamforming optimization," *IEEE Transactions on Communications*, 2020.

31. Zhu, F.; Wang, X.; Huang, C.; Yang, Z.; Chen, X.; Al, H. Ahmed Robust Beamforming for RIS-Aided Communications: Gradient-Based Manifold Meta Learning *IEEE Transactions on Wireless Communications* **2024**, *23*, *11*, 15945-15956.

32. Wang, X.; Zhu, F.; Huang, C.; Yang, Z.; Chen, X.; Al, H. Ahmed Robust Beamforming With Gradient-Based Liquid Neural Network *IEEE Transactions on Wireless Communications* **2024**, *23*, *11*, 15945-15956.